# Mud-crack size distributions in soils and their relationship with soil properties

Mud cracks form due to the desiccation of water-saturated soil and other clayey sediments. Several experimental works done with drying synthetic and natural clay reveal that the coalescence of smaller cracks and repetitive moistening and drying of muds lead to the self-similar nature of the mud cracks[1–4]. This paper presents a study on the mud cracks in soil developed under natural conditions and quantify the frequency distributions of their geometrical parameters like perimeter ($P$) and crack enclosed area ($A$) that define the size of a mud crack. The dependence of the derived 'frequency distribution coefficients ($D$)' on physical soil substrate parameters like moisture content clay content, and gross chemical composition are studied. The moisture content of the substrate soil together with the abundance of grass seems to play pivotal roles in defining the mud crack size distribution.

Mud cracks are shallow-water sedimentary features with interconnected polygonal crack network formed as a consequence of gradual drying of soil patches as well as other muddy sediments. The polygonal area enclosed by an individual mud crack is usually quadrilateral or hexagonal. However, other unusual patterns are also reported in the literature, viz. radiate, rectangular or incomplete cracks[2]. Their shapes represent the terrain steepness on which they form. Mud cracks with quadrilateral or rectangular morphology are termed as rectangular cracks and the ones with polygonal shapes are called reticular cracks (netlike)[3]. Mechanically, maximum principal tensile strain triggers the initiation of a crack and more desiccation leads to the propagation of the cracks[4,5]. The mudcrack morphology in soil and its formation are generally influenced by several physical and chemical factors. Some organisms burrow the soil substrate and produce secondary cracks which are also accounted as mud cracks[3], presence of microbial mat leads to the higher degree of curving than normal mud cracks[6]. Fine sand content in a significant amount in the soil and slow pace of drying facilitate the profuse development of wider polygonal mud cracks. On the contrary, any mixture of clay and marl with a rapid drying rate create closely spaced polygonal cracks[7].

The geometrical parameters commonly used to characterize mud cracks size are crack perimeter ($P$), crack area (polygonal area limited by the crack surface; $A$), crack width or aperture, penetration depth ($d$) and the angle between two consecutive crack sides of the polygon. However, here we focus on the perimeter and crack area as representatives of crack size and test if their frequency ($N$) of occurrences vary with size[8,9]. Similar statistical tests are done to define if the occurrence of a physical phenomenon follows 'fractal' distribution which is a scale invariance[10] geometry that tends to exhibit self-similarity[11]. It is generally characterized by Power Law frequency distribution and quantified by the 'fractal dimension'. A number of natural phenomena are known to follow a fractal distribution, such as the frequency of earthquakes of various sizes, clast sizes in the rock fragments or the dendritic branching of the stream channel[12], etc. Although we have not specifically tested if the mud cracks size distributions follow fractal rules, we have used the size-frequency distribution coefficients as representatives of mud crack size distribution for a particular population and tested their dependence on physical soil substrate parameters.

The ordinary appearance of mud crack reveals complex patterns when studied in detail. We studied mud cracks developed naturally on the open soil inside the IISER Bhopal campus (Figure 1 a). The basic rock types around the Bhopal area are Vindhyan sandstone and Deccan Basalt[13]. The weathered material from such rocks collectively forms the soil. Five different study sites were selected. In a given site, we divided the area into multiple grids of 1 m × 1 m dimension (Figure 1 b) and measured the penetration depths ($d$) of the cracks. The other physical parameters such as area ($A$) and perimeter ($P$) of the polygonal cracks (Figure 1 c) were estimated from the scaled digital photograph (captured orthogonally) using the 'ImageJ' software. Additionally, soil surface samples were collected for the measurement of other properties such as moisture, clay content and bulk chemical composition. Moisture content ($M$) was measured by calculating the difference in weight between an insitu sample and dried sample using hot air at 40°C. The sample was dried a few times till the weight of the sample no longer changed ensuring complete desiccation. Clay content ($C$) was measured after the successful separation of clay from the soil samples (by creating vortex in water saturated with soil sample that suspends clay particles in water which upon centrifugation separates it) and the powdered X-ray diffraction (XRD) analysis was applied (which produces peaks at each wave interference pattern for the present chemical compounds) for clay composition.

Figure 1 d shows a histogram displaying the cumulative frequency distribution of the crack area for a particular location. It shows that the smaller cracks occur more frequently in number than the larger ones. With increasing desiccation in the soil which induces soil maturity, soil moisture decreases and thermal stress increases. This leads to the formation of new smaller cracks as well as coalescence of existing smaller cracks into larger cracks.

In another representation of the same data, the cumulative frequency was plotted against the crack area in the log–log scale (Figure 1 e). The scatter plot reveals that the data can be broadly subdivided into two groups: (a) for very small crack size, cumulative frequency increases with crack size, (b) after a threshold crack size, the cumulative frequency decreases with crack size, perhaps portraying fractal behaviour. The former group of data, most likely, represents an 'under-sampled' data cloud due to the low spatial resolution of the measurement. Frequency distribution ($D$) was calculated for the latter group by calculating the negative slope of the linear trendline. The same methodology was repeated for all five locations and $D$ representing each location's mud crack population were calculated and are listed in Table 1. The measured crack perimeter ($P$) was also tested with the same statistical analysis approach (Figure 1 f and g) and corresponding $D$ values were calculated (also listed in Table 1).

**Table 1.** Soil analysis data and mud crack size distribution frequency coefficients

| Location | M (%) | C (%) | $D_A$ | $D_P$ | Carbonate/silica ratio |
|---|---|---|---|---|---|
| 1 | 1 | 0.6138 | −3.4292 | −5.6488 | 1.5882 |
| 2 | 1.06 | 0.6225 | −2.794 | −4.6555 | 0.5151 |
| 3 | 2.36 | 0.6736 | −1.2912 | −2.6572 | 0.0869 |
| 4 | 2.42 | 0.6786 | −1.1731 | −2.9369 | 0.5873 |
| 5 | 7.29 | 0.8652 | −2.8639 | −5.3763 | 0.0638 |

M, Moisture; C, Clay content; $D_A$, Crack area frequency distribution coefficient; $D_P$, Crack perimeter frequency distribution coefficient.
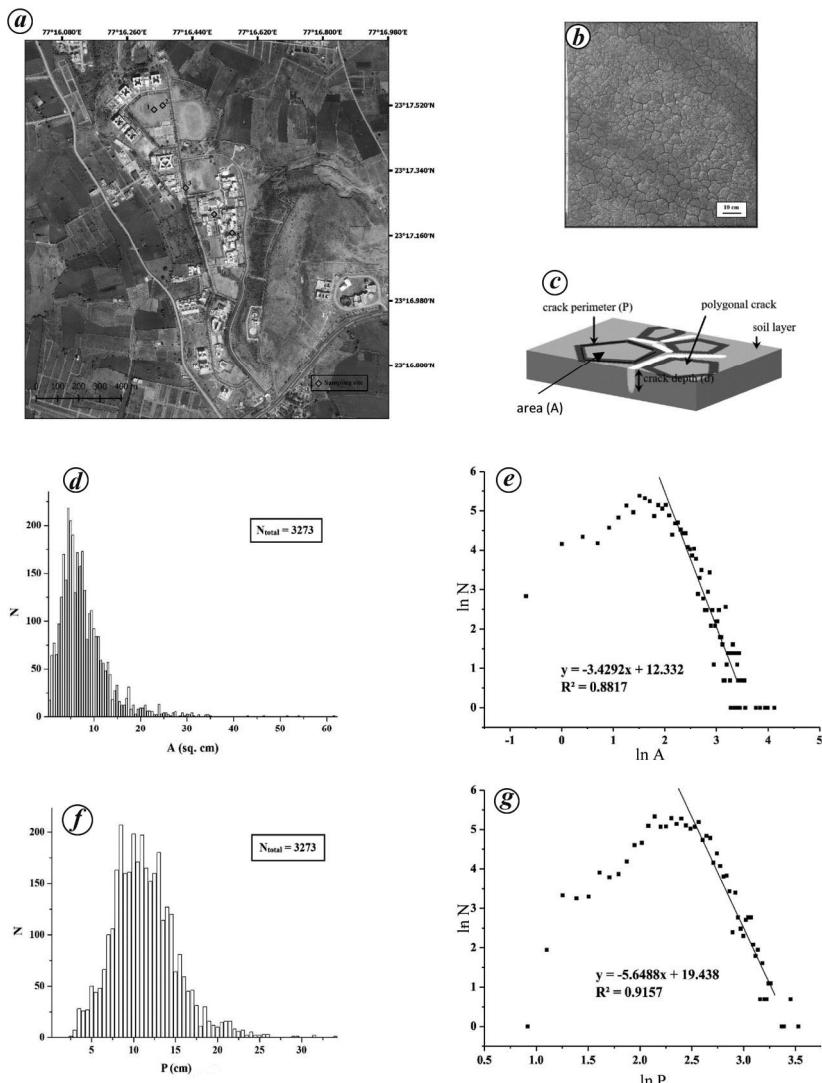


**Figure 1.** *a*, Google satellite image showing sites of study in IISER Bhopal campus. *b*, Field photograph showing exposed mud cracks at location 1. *c*, Schematic diagram showing mud crack area, perimeter and depth. *d*, Histogram showing frequency distribution of enclosed mud crack area in sq. cm (A). *e*, Scatter plot of A against frequency in log–log scale and the slope of linear trendline ($D_A$). *f*, Histogram showing frequency distribution of mud crack perimeter in cm (P). *g*, A scatter plot of perimeter against frequency in log–log scale and the slope of linear trendline ($D_B$).

No obvious correlation was found between mean penetration depth (calculated by measuring depths of a polygonal crack inserting a ruler inside at different parts of the crack) and crack area or crack perimeter (Figure 2 *a* and *b*).

Calculated moisture percentage, clay content, and carbonate to silica ratio ($CaO + CO_2/SiO_2$) as calculated from XRD analysis of the soil samples are also listed in Table 1. The XRD measurements were performed using a PANalytical Empyrean X-ray diffractometer in the Bragg-Brentano geometry using a Cu–$K_{\alpha 1}$ (wavelength = 1.5405 Å) line focused radiation and Ni beta filter was used to obtain the $K_\alpha$ (to remove $K_{beta}$) radiation. The powder samples were mounted on the silicon zero background holder by dropping powder and then flat the sample surface with a glass plate. The generator power sets at 45 kV and 40 mA to measure the powder X-ray data. The data were collected using the Pixcel[3D] detector in the angular range of 10° to 80° in the $2\theta$ range within steps of 0.013°. The soil sample contains some clay mineral but XRD method determines chemical components that show presence of Ca-bearing compound in the form of $CaCO_3$ and quartz and so it is represented as distinct carbonate to silica ratio. Moisture content increases linearly with the amount of clay present in the soil (Figure 2 *c*) indicating the increase in moisture-retaining capacity in soil with an increase in clay. In clay-rich soils, polygonal cracks are widely spaced compared to the sand-rich soil in the initial stages of crack formation[7].

Figure 2 *d* shows a plot between frequency distribution coefficients (*D*) of crack area (*A*) and the calculated moisture percentage of the same location. The plot reveals that the *D* value (both for perimeter and crack area) increases with a decrease in moisture content except for location 5. This suggests that a drier soil being more mature shows greater 'heterogeneity'[9] in crack size distribution and smaller cracks are favoured in drier soil and relatively larger cracks are favoured in wet soil. The deviation from the general trend at location 5 is perhaps because of the abundance of grass in the location affecting the development of mud cracks. With the increase in carbonate to silica ratio, *D* values seem to increase but the observed correlation is weak (Figure 2 *e*) and will require more data points to comment further.

The presented correlations will be particularly important while analysing palaeo mud cracks. With more data points, better-constrained correlations can be established between soil parameters and mud crack size distributions. Once such
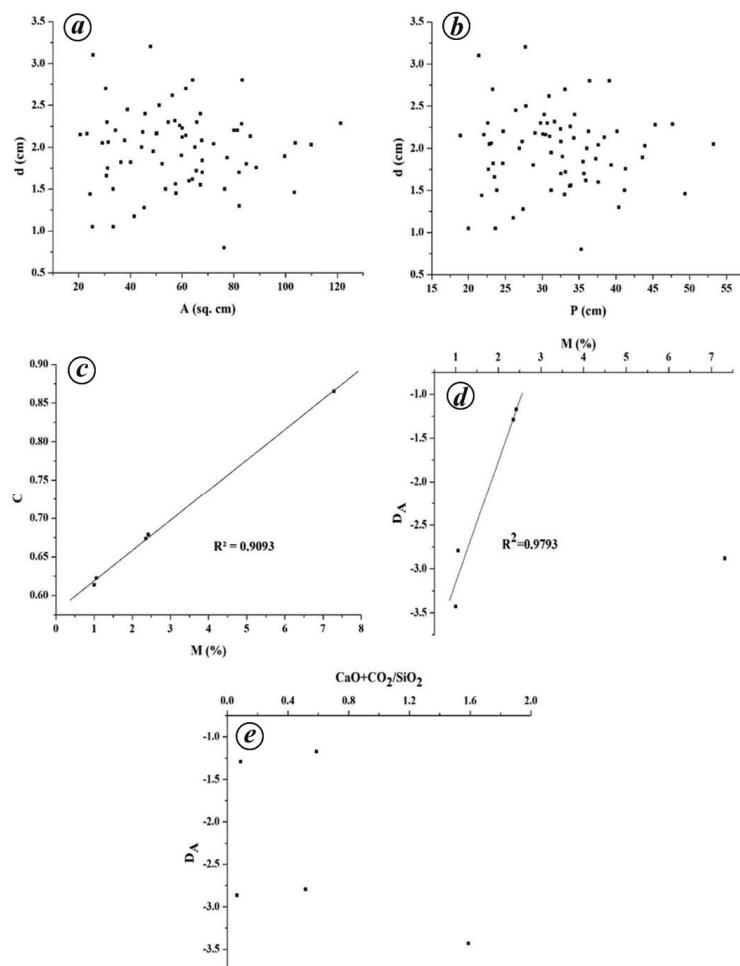
5. Morris, P. H., Graham, J. and Williams, D. J., *Can. Geotech. J.*, 1992 online; doi:10.1139/t92-030.
6. Porada, H., In *Encyclopedia of Earth Sciences Series*, 2011; doi:10.1007/978-1-4020-9212-1_148.
7. Kindle, E. M., *J. Geol.*, 1917 online; doi:10.1086/622446.
8. Khatun, T., Dutta, T. and Tarafdar, S., *Eur. Phys. J. E.*, 2015 online; doi:10.1140/epje/i2015-15083-6.
9. Preston, S., Griffiths, B. S. and Young, I. M., *Eur. J. Soil Sci.*, 1992 online; doi:10.1111/j.1365-2389.1997.tb00182.x.
10. Mandelbrot, B. B. and Wheeler, J. A., *Am. J. Phys.*, 1983 online; doi:10.1119/1.13295.
11. Boeing, G., *Systems*, 2016 online; doi:10.3390/systems4040037.
12. Turcotte, D. L., *PAGEOPH*, 1989 online; doi:10.1007/BF00874486.
13. Balakrishna, S., *Bull. Volcanol.*, 1967 online; doi:10.1007/BF02597651.

**Figure 2.** *a*, Scatter plot of crack area against the crack depth showing no apparent correlation (shown for location 1). *b*, Scatter plot of crack perimeter against crack depth showing no apparent correlation (shown for location 1). *c*, Scatter plot of soil moisture against the clay content showing positive correlation between them. *d*, Scatter plot of moisture versus $D_A$. *e*, A scatter plot of carbonate to silica ratio against the $D_A$ showing a weak correlation.

robust correlations are established, scientists should be able to comment on the moisture content and chemical compositions of the palaeosols from size distributions of the mud crack populations. Such inferences could provide additional ways of constraining palaeo-climate. The other important area where observed correlations can be effectively used is agriculture as the size of the mud crack population defines the permeability of the topsoil, facilitating the flow of the irrigation water and constrains the contamination of groundwater by arsenic or similar hazardous chemicals.

1. Goehring, L., *Philos. Trans. R. Soc. A Math. Phys. Eng. Sci.*, 2013 online; doi:10.1098/rsta.2012.0353.
2. Zhao, Z. Y., Zhou, Y. Q. and Ma, X. M., *Xi'an Shiyou Daxue Xuebao (Ziran Kexue Ban)/Journal Xi'an Shiyou Univ. Nat. Sci. Ed.*, 2008 online.
3. Zhao, Z. yu., Guo, Y. ru., Wang, Y., Liu, H. and Zhang, Q., *Int. J. Sediment. Res.*, 2014 online; doi:10.1016/S1001-6279(14)60024-X.
4. Hirose, K. and Matsubara, H., *J. Geotech. Geoenviron. Eng.*, 2018 online; doi:10.1061/(ASCE)GT.19435606.0001-853.

RAJPUT MITESH RAKESHBHAI[1]
JYOTIRMOY MALLIK[1,]*
SUDIP CHUNARY[1]
D. SHRINIVASH[2]
JAYA SINGH[3]

[1]Indian Institute of Science Education and Research,
Bhopal 462 066, India
[2]Manipal Academy of Higher Education, Manipal 576 104, India
[3]Indian Institute of Technology, Roorkee 247 667, India
*For correspondence.
e-mail: jmallik@iiserb.ac.in